Solid State Communications 250 (2017) 1–4

Contents lists available at ScienceDirect

Solid State Communications

journal homepage: www.elsevier.com/locate/ssc

Communication

Gd-doping-induced insulator-metal transition in $SrTiO_3$

Yanni Gu[a,b], Sheng Xu[a,b], Xiaoshan Wu[a,*]

[a] National Laboratory of Solid State Microstructures and Department of Physics, Nanjing University, Nanjing 210093, China
[b] Zhangjiagang Campus, Jiangsu University of Science and Technology, Zhangjiagang 215600, China

ARTICLE INFO

Keywords:
Insulator-metal transition
Ferrimagnetism
Gd-doping
Density-function theory

ABSTRACT

Recently, insulator-metal transition was found experimentally in Gd-doped $SrTiO_3$ films. Here, we present first-principle investigation on the structural, electronic and magnetic properties of $Sr_{1-x}Gd_xTiO_3$ within density-function theory. The spin-polarized calculations give a diamagnetic insulator at x=0, a ferrimagnetic metal $0.125 \leq x \leq 0.5$ and a ferrimagnetic insulator x=1 and all Ti ions moments are antiparallel to Gd ions moments. Magnetic Gd-doping distorts the structures of $Sr_{1-x}Gd_xTiO_3$ films and results in ferrimagnetism. Doped electrons occupy the bottom of conduction bands so that insulator-metal transition occurs. These calculated results are in agreement with available experiments.

1. Introduction

$SrTiO_3$ is a band insulator, which has a 3.2 eV band gap [1]. It is used widely as thermoelectric devices [2], memory devices [3] and piezoelectric devices [4]. And it has attracted extensive attention owing to many fascinating phenomena it displayed such as ferromagnetism [5], superconductivity [6], structure phase transition [7], two-dimensional electron gas [8], etc.

Conductor electrons were drawn into $SrTiO_3$ when transition-metal oxides were grown on $SrTiO_3$ such as $LaAlO_3/SrTiO_3$ superlattices [9,10]. Additionally, conductor electrons in $SrTiO_3$ can be induced by oxygen vacancy [11] and substitutional rare-earth ions doping [12–17]. $SrTiO_3$ with oxygen vacancy underwent insulator-metal transition [11], which was tempted by the carrier freeze-out effect. Partial substitution in Sr sites with La atoms in $SrTiO_3$ generated a strongly correlated metal phase [17]. The optically doped $SrTi_{1-x}Nb_xO_3$ was identified as a multi-band s-wave superconductor [12]. Cr doping in $SrTiO_3$ resulted in insulator-metal transition [18]. Recently, insulator-metal transition also occurred in Gd-doped $SrTiO_3$ or Sr-doped $GdTiO_3$ and a ferrimagnetic metal phase was found [16]. Due to the characteristic of insulator-metal transition in doped $SrTiO_3$, $SrTiO_3$ has promising applications such as memory device, etc. This makes it important to understand theoretically the nature of insulator-metal transition in doped $SrTiO_3$.

In order to understand the experimentally-observed insulator-metal transition and ferrimagnetism in Gd-doped $SrTiO_3$ films [16], we made first-principle calculations on the structural, electronic and magnetic properties of $Sr_{1-x}Gd_xTiO_3$ within density-function theory (DFT) based on generalized gradient approximation plus U (GGA + U). The present theoretical results match with available experimental evidence. We interpret well the phenomenon of insulator-metal transition in $Sr_{1-x}Gd_xTiO_3$ and reveal the origin of ferrimagnetism.

2. Calculation detail

The first-principle calculations of $Sr_{1-x}Gd_xTiO_3$ (x=0, 0.125, 0.25, 0. 5 and 1) were performed within DFT based on a projector-augmented wave (PAW) [19] potentials as implemented in Vienna ab-inito simulation package (VASP) [20]. For the exchange-correlation functions, we used GGA+U with the Perdew-Burke-Ernzerhof (PBE) scheme. All calculations were performed with the Hubbard U=5.0 and an approximation of the Stoner exchange parameter J=0.64 applied on d-orbitals of Ti atoms [21]. First, bulk $SrTiO_3$ and $GdTiO_3$ were fully relaxed. A 40-atom $SrTiO_3$ supercell with size 2×2×2 and a 20-atom $GdTiO_3$ unit cell were used for calculations. Next, $Sr_{1-x}Gd_xTiO_3$ ($0 < x \leq 0.5$) films were fully optimized. A few of Sr atoms in $SrTiO_3$ supercell were substituted by Gd atoms to calculate $Sr_{1-x}Gd_xTiO_3$ films. In order to reproduce experiment results [16], the parameters in ab plane were fixed as 7.810 Å, two times of the experimental lattice parameter of $SrTiO_3$ substrate [22]. The lattice parameter along c axis and all atom positions were fully optimized in $Sr_{1-x}Gd_xTiO_3$ ($0 < x \leq 0.5$) films. The plane-wave energy cutoff for the electrons was 400 eV. A 5×5×5 grid of Monkhorst–Pack mesh was used for the k-point sampling in $Sr_{1-x}Gd_xTiO_3$ ($0 \leq x \leq 0.5$) and A 8×8×6 grid in $GdTiO_3$. Six electrons ($2s^22p^4$), ten electrons ($4s^24p^65d^2$), four electrons ($3d^34s^1$) and eighteen electrons $4d^75^25p^65d^16s^2$, treated as valence electrons, were for

* Corresponding author.
E-mail address: xswu@nju.edu.cn (X. Wu).

http://dx.doi.org/10.1016/j.ssc.2016.11.013
Received 15 October 2016; Accepted 13 November 2016
Available online 14 November 2016

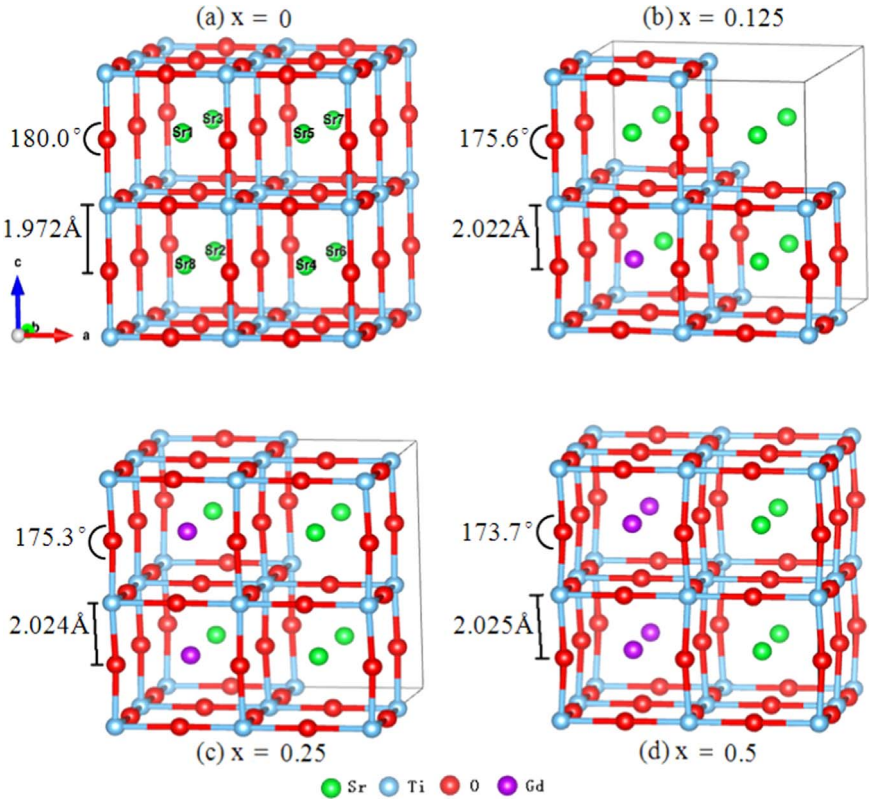

Fig. 1. (Color online) Optimized structures of bulk $SrTiO_3$ (x=0) and $Sr_{1-x}Gd_xTiO_3$ films (0 < x≤0.5): (a) x=0, (b) x=0.125, (c) x=0.25 and (d) x=0.5.

Table 1
The lattice parameters, band gaps and magnetic ground states of $SrTiO_3$ and $GdTiO_3$.

	$SrTiO_3$		$GdTiO_3$work	
	Experiment	This work	Experiment	This work
a(Å)	3.905[22]	3.945	5.403[23]	5.437
b(Å)	3.905	3.945	5.701	5.782
c(Å)	3.905	3.945	7.674	7.737
band gap(eV)	3.22[1]	2.35	> 0[26]	1.90
the magnetic ground state	diamagnetic[24]	diamagnetic	ferrimagnetic[25]	ferrimagnetic

Table 2
Magnetic moment at atom sites in the ground state of bulk $SrTiO_3$ and $Sr_{1-x}Gd_xTiO_3$ films.

$Sr_{1-x}Gd_xTiO_3$	Atom sites	magnetic moments (μ_B)
x=0	Ti	0
x=0.125	Ti	−0.036
	Gd	6.801
x=0.25	Ti	−0.246
	Gd	6.785
x=0.5	Ti	−0.446
	Gd	6.747
x=1	Ti	−0.958
	Gd	6.897

the O, Sr, Ti and Gd atoms, respectively. Between successive iterations the electronic calculations were converged to 10^{-5} eV, and the Hellman-Feynman force calculations were converged to less than 10^{-4} eV/Å.

3. Results and discussion

3.1. Structure relaxation and magnetic properties

First, the structures of bulk $SrTiO_3$ and $GdTiO_3$ were optimized. $SrTiO_3$ is a typical cubic structure with Pm-3m space group [22] while $GdTiO_3$ has a highly distorted perovskite structure with Pbnm space group [23]. The experimental lattice parameter a=3.905 Å is for $SrTiO_3$ [22] and a=5.403, b=5.701, and c=7.674 [23] are for $GdTiO_3$. As shown in Fig. 1(a), TiO_6 octahedral has a cubical structure where Ti atom is at the center and O atoms are at the ends of the edges. The parameters a, b and c, the ground states and band gaps are listed in Table 1. The calculated lattice parameters of a=3.945 Å for $SrTiO_3$ and a=5.437 Å, b=5.782 Å and c=7.737 Å for $GdTiO_3$ are in reasonable accordance with the previous experimental values [22,23]. The ground states of $SrTiO_3$ and $GdTiO_3$ are diamagnetic and ferrimagnetic insulators, respectively, in agreement with experimental results [1,24–26]. The total energy of A, G and C-type antiferromagnetic configuration of $GdTiO_3$ are higher than the ferrimagnetic structure by 0.05, 0.81 and 0.82 eV per formula. Ferromagnetic $GdTiO_3$ converges to ferrimagnetic state, where all Ti ions moments are antiparallel to those of Gd ions. As shown in Table 2, the calculated magnetic moments in $GdTiO_3$ are $-0.958\mu_B$/Ti and $6.897\mu_B$/Gd.

Second, $Sr_{1-x}Gd_xTiO_3$ films (x=0.125, 0.25 and 0.5) were calculated. The present calculated results show that the ground states of the $Sr_{1-x}Gd_xTiO_3$ films are ferrimagnetic, where all moments of Ti ions are antiparallel to those of Gd ions. In order to reproduce experimental results [16], the parameters within the ab plane were fixed as 7.810 Å, namely, two times of the experimental lattice parameter a of $SrTiO_3$ substrate. Then the lattice parameter along c axis and all atom positions are fully optimized. All optimized structures of the ground states in $Sr_{1-x}Gd_xTiO_3$ films (x=0.125, 0.25 and 0.5) are shown in Fig. 1. Green, blue, red and purple spheres represent Sr, Ti, O and Gd atoms, respectively. Three different types [27] of structures were modeled for $Sr_{0.75}Gd_{0.25}TiO_3$, which were constructed by substituting

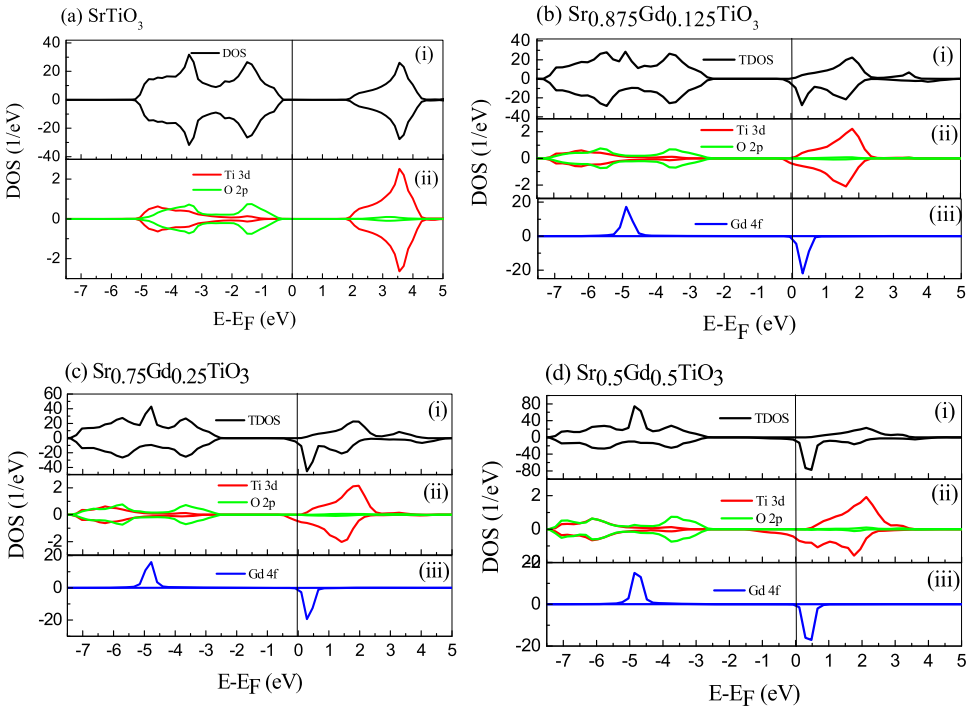

Fig. 2. (Color online) Total Density of States (TDOS) and partial DOS (PDOS) of $Sr_{1-x}Gd_xTiO_3$: (a) x=0, (b) x=0.125, (c) x=0.25, and (d) x=0.5.

two Sr atoms using two Gd atoms at positions (Sr1, Sr8) (see Fig. 1(c)), (Sr5, Sr8) and (Sr7, Sr8), respectively. Five kinds of structures were modeled for $Sr_{0.5}Gd_{0.5}TiO_3$, which were constructed by substituting four Sr atoms using four Gd atoms at positions (Sr1, Sr2, Sr3, Sr8) (see Fig. 1(d)), (Sr1, Sr2, Sr4, Sr6), (Sr1, Sr2, Sr4, Sr8), (Sr1, Sr2, Sr7, Sr8) and (Sr3, Sr5, Sr6, Sr8), respectively. For each kind of structure of $Sr_{1-x}Gd_xTiO_3$ films (x=0.125, 0.25 and 0.5), we calculated ferromagnetic and antiferromagnetic configurations [28] and found that the ground state is ferromagnetic and ferromagnetic configuration converged to ferrimagnetic one. For ferrimagnetic configuration in all the kinds of structures in $Sr_{0.75}Gd_{0.25}TiO_3$ and $Sr_{0.5}Gd_{0.5}TiO_3$ films, the total energy of the structures in Fig. 1(c) for x=0.25 and Fig. 1(d) for x=0.5 are the lowest, respectively. As is shown in Fig. 1, the Ti-O-Ti angle decreases and thereby distorted structures occur while Ti-O bond length increases slightly as Gd concentration increases. The space groups for x=0, 0.125, 0.25 and 0.5 are Pm-3m, Amm2, P4/mmm and Pmmm, respectively, which are determined through FINDSYM software [29]. Obviously, the structures of $Sr_{1-x}Gd_xTiO_3$ films change due to Gd-doping. It is able to test our prediction to measure further experimentally the $Sr_{1-x}Gd_xTiO_3$ structures. Also, doping-induced structural phase change was experimentally found in Nd-doped $EuTiO_3$ [30].

Ti and Gd atom moments of the ground state are listed In Table 2. Table 2 does not display the O and Sr moments of 0 μ_B. According to Table 2, $Sr_{1-x}Gd_xTiO_3$ films show clear ferrimagnetic properties as the negative moments of Ti are antiparallel to the positive moments of Gd. The total moments of $Sr_{1-x}Gd_xTiO_3$ are 0 μ_B, 6.513 μ_B, 11.608 μ_B and 23.48 μ_B at x=0, 0.125, 0.25 and 0.5, respectively. Experimentally, ferrimagnetism decreased monotonically in $Sr_{1-x}Gd_xTiO_3$ ($x > 0.5$) films as x decreases [16]. The change trend of experimental ferrimagnetism is as similar as that of the total magnetic moments in the present calculation. Experimental result on $Sr_{0.44}Gd_{0.56}TiO_3$ film [16] showed clear ferrimagnetic properties below 30 K, which is in agreement with the present theoretical results. Magnetic Gd-doping drives the system from the diamagnetic to the ferrimagnetic.

3.2. Electric structure

The present GGA+U calculations give an insulator ground state at x=0 and a metal ground state at x=0.125, 0.25 and 0.5 in $Sr_{1-x}Gd_xTiO_3$, which agree well with the experimental results [16]. The calculated total densities of states (TDOS) and the partial DOS (PDOS) of Ti 3d, O 2p and Gd 5f of the ground state in Fig. 1 are shown in Fig. 2(a)–(d). For x=0.25 and 0.5, TDOS and PDOS of the ferrimagnetic configuration in the additional structures are as similar as those in Fig. 2. The energy window in the present discussion is limited from −7.5 to 5 eV and the Fermi energy is zero. The PDOS of Ti 3d, O 2p and Gd 4f are mainly concerned with but that of Sr is ignored because the value and conduction bands of $Sr_{1-x}Gd_xTiO_3$ do not derive from Sr states.

$SrTiO_3$ is known as a diamagnetic insulator at room temperature [1,24], which is consistent with the present DOS calculations. The calculated TDOS and PDOS of $SrTiO_3$ as displayed in Fig. 2(a) are as similar as the previous theoretical results [27,31]. Two groups of states are recognized. The fully occupied states of $SrTiO_3$ are dominated mainly by Ti 3d and O2p orbitals while the unoccupied states are dominated mainly of Ti 3d orbitals. The calculated band gap at Γ point is 2.35 eV, which is bigger than the previous theoretical [27,31] values and smaller than the experiment value, 3.22 eV [1], due to the famous limitation of the GGA scheme.

The situation changes rapidly on turning to the $Sr_{1-x}Gd_xTiO_3$ films. TDOS and PDOS of $Sr_{0.875}Gd_{0.125}TiO_3$ film are displayed in Fig. 2(b). Experimentally, the $Sr_{0.875}Gd_{0.125}TiO_3$ film is a metal [16], which is consistent with the present calculations. The O 2p bands locate at from ~−7.17 eV to ~−2.32 eV. The Ti 3d bands located at from ~−7.11 eV to ~−2.67 eV and from ~−0.23 eV to ~2.53 eV. The spin-up Gd 4f bands span from ~−5.25 eV to ~−4.31 eV and spin-down from ~−0.14 eV to ~0.75 eV. The valence bands are dominated mainly by Ti 3d and O 2p state but the conduction bands are dominated mainly of Ti 3d and Gd 4f states. The spin-down bands of Gd 4f and Ti 3d straddle the Fermi level, resulting in a metal ground state. It is clearly seen that doped electrons occupy the bottom of conduction bands due to substitutional Gd and thereby the Fermi level moves upwards into conduction bands. The total DOS is ~−7.72 states/eV at the Fermi level. This further confirms that Gd-doped $SrTiO_3$ experiences insulator -metal transition.

Finally, $Sr_{1-x}Gd_xTiO_3$ (x=0.25 and 0.5) films are considered. We find the striking similarity to the total DOS of $Sr_{0.875}Gd_{0.125}TiO_3$ film as connected with width and shape, the primary difference is that sharp peaks derived from Gd states become higher since ferrimagnetism becomes strong as x increases. The present calculation results also display that $Sr_{0.75}Gd_{0.25}TiO_3$ and $Sr_{0.5}Gd_{0.5}TiO_3$ are still metal, which agrees with the experimental results [16].

4. Conclusion

In conclusion, we study the structural, electronic and magnetic properties of Gd-doped $SrTiO_3$ (x=0, 0.125, 0.25, 0.5 and 1) based on first-principle calculations. We find the ground state of $Sr_{1-x}Gd_xTiO_3$ film is ferrimagnetic and Gd doping results in insulator-metal transition. The present theoretical results interpret well recently experimentally-observed insulator-metal transition.

Acknowledgement

We are thankful for the financial support from the National Natural Science Foundation of China (Nos. U1332205, 11274153 and 11204124) and Jiangsu Province Postdoctoral Fund (No. 1301019B). We are grateful to the High Performance Computing Center of Nanjing University and Jiangsu University of Science and Technology for the award of CPU hours.

References

[1] J.A. Noland, Phys. Rev. **94** (1954) 724.
[2] H. Ohta, S. Kim, Y. Mune, T. Mizoguchi, K. Nomura, S. Ohta, T. Nomura, Y. Nakanishi, Y. Ikuhara, M. Hirano, H. Hosono, K. Koumoto, Nat. Mater. **6** (2007) 129.
[3] A. Mottaghizadeh, Q. Yu, P.L. Lang, A. Zimmers, H. Aubin, Phys. Rev. Lett. **112** (2014) 066803.
[4] K. Morito, Y. Iwazaki, T. Suzuki, M. Fujimoto, J. Appl. Phys. **94** (2003) 5199.
[5] J.A. Bert, B. Kalisky, C. Bell, M. Kim, Y. Hikita, H.Y. Hwang, K. a Moler, Nat. Phys. **7** (2011) 767.
[6] J.F. Schooley, W.R. Hosler, M.L. Cohen, Phys. Rev. Lett. **12** (1964) 474.
[7] G. Shirane, Y. Yamada, Phys. Rev. **177** (1969) 858.
[8] A.F. Santander-Syro, O. Copie, T. Kondo, F. Fortuna, S. Pailhès, R. Weht, X.G. Qiu, F. Bertran, A. Nicolaou, A. Taleb-Ibrahimi, P. Le Fèvre, G. Herranz, M. Bibes, N. Reyren, Y. Apertet, P. Lecoeur, A. Barthélémy, M.J. Rozenberg, Nature **469** (2011) 189.
[9] L. Li, C. Richter, J. Mannhart, R.C. Ashoori, Nat. Phys. **7** (2011) 762.
[10] A. Ohtomo, H.Y. Hwang, Nature **441** (2004) 120.
[11] Z.Q. Liu, D.P. Leusink, X. Wang, W.M. Lü, K. Gopinadhan, A. Annadi, Y.L. Zhao, X.H. Huang, S.W. Zeng, Z. Huang, A. Srivastava, S. Dhar, T. Venkatesan, Ariando, Phys. Rev. Lett. **107** (2011) 146802.
[12] X. Lin, C.W. Rischau, C.J. van der Beek, B. Fauqué, K. Behnia, Phys. Rev. B **92** (2015) 174504.
[13] Z. Guguchia, A. Shengelaya, H. Keller, J. Köhler, A. Bussmann-Holder, Phys. Rev. B **85** (2012) 134113.
[14] G. Binnig, A. Baratoff, H.E. Hoenig, J.G. Bednorz, Phys. Rev. Lett. **45** (1980) 1352.
[15] A. Spinelli, M.A. Torija, C. Liu, C. Jan, C. Leighton, Phys. Rev. B **81** (2010) 155110.
[16] P. Moetakef, T.A. Cain, Thin Solid Films **583** (2015) 129.
[17] Y. Tokura, Y. Taguchi, Y. Okada, Y. Fujishima, T. Arima, K. Kumagai, Y. Iye, Phys. Rev. Lett. **70** (1993) 2126.
[18] G.I. Meijer, U. Staub, M. Janousch, S.L. Johnson, B. Delley, T. Neisius, Phys. Rev. B **72** (2005) 155102.
[19] G. Kresse, D. Joubert, Phys. Rev. B **59** (1999) 1758.
[20] G. Kresse, J. Furthmüller, Phys. Rev. B **54** (1996) 11169.
[21] E. Pavarini, S. Biermann, A. Poteryaev, A.I. Lichtenstein, A. Georges, O.K. Andersen, Phys. Rev. Lett. **92** (2004) 176403.
[22] S.A. Howard, J.K. Yau, H.U. Anderson, J. Appl. Phys. **65** (1989) 1492.
[23] A.C. Komarek, H. Roth, M. Cwik, W.D. Stein, J. Baier, M. Kriener, F. Bour??e, T. Lorenz, M. Braden, Phys. Rev. B - Condens. Matter Mater. Phys. **75** (2007).
[24] H. Trabelsi, M. Bejar, E. Dhahri, M. Sajieddine, M.A. Valente, A. Zaoui, J. Alloys Compd. **680** (2016) 560.
[25] H.D. Zhou, J.B. Goodenough, J. Phys. Condens. Matter **17** (2005) 7395.
[26] P. Moetakef, D.G. Ouellette, J.Y. Zhang, T.A. Cain, S.J. Allen, S. Stemmer, J. Cryst. Growth **355** (2012) 166.
[27] A. Kinaci, C. Sevik, T. Çağın, Phys. Rev. B **82** (2010) 155114.
[28] E.O. Wollan, W.C. Koehler, Phys. Rev. **100** (1955) 545.
[29] See, ⟨http://stokes.byu.edu/findsym.html⟩.
[30] L. Poudel, C. de la Cruz, E.A. Payzant, A.F. May, M. Koehler, V.O. Garlea, A.E. Taylor, D.S. Parker, H.B. Cao, M.A. McGuire, W. Tian, M. Matsuda, H. Jeen, H.N. Lee, T. Hong, S. Calder, H.D. Zhou, M.D. Lumsden, V. Keppens, D. Mandrus, A.D. Christianson, Phys. Rev. B **92** (2015) 214421.
[31] S. Carlotto, M.M. Natile, A. Glisenti, A. Vittadini, Chem. Phys. Lett. **588** (2013) 102.